Electronic Supplementary Material (ESI) for CrystEngComm.

SUPPORTING INFORMATION

Lanthanide-based molecular alloys with hydroxy-terephthalate: A versatile system.

Jinzeng Wang, Yan Suffren, Carole Daiguebonne, Kevin Bernot, Guillaume Calvez, Stéphane Freslon and Olivier Guillou*.

Univ Rennes, INSA Rennes, CNRS UMR 6226 "Institut des Sciences Chimiques de Rennes", F-35708 Rennes, France.

* To whom correspondence should be addressed: Olivier.guillou@insa-rennes.fr

Synthesis of the di-sodium salt of 2-hydroxy-terephthalic acid.

A stoichiometric amount of sodium hydroxide is added to an aqueous suspension of H_2hbdc under stirring. The obtained clear solution is evaporated to dryness. The collected solid is dissolved in ethanol and refluxed for 1 h. Precipitation is provoked by addition of an excess of diethyl ether. The white precipitate is filtered and washed with diethyl ether. After recrystallization in deionized water, the powder is collected and dried under ambient temperature and pressure conditions. The yield is about 90%. Despite great efforts we didn't succeed in obtaining single crystals. Thermal analyses indicate that the compound is once hydrated. (Figure S1) Elemental analysis of $Na_2(hbdc)\cdot H_2O$: $Na_2C_8H_6O_6$ MW = 244 g.mol^{-1}. Found (calc.). Na: 19 % (18.8 %), C: 39.0 % (39.3 %), H: 2.8 % (2.6 %), O: 39.2 % (39.3 %).

Synthesis of the single-crystals of the coordination polymers

Three different synthetic methods have been used to grow single-crystals.

(i) Solvo-thermal method: 0.1 mmol of a lanthanide chloride, 0.15 mmol of H_2hbdc, 6 mL of H_2O and 200 µL of an aqueous solution of sodium hydroxide (1 mol.L^{-1}) were placed in a 24 mL Parr autoclave. Parr autoclave was heated at 110°C during 4 days and then cooled to room temperature at a rate of 3°C.h^{-1}. The obtained transparent single-crystals were filtered and dried at ambient conditions. Three different crystal structures were obtained by this method (structural families **F2**, **F3** and **F4**).

(ii) Slow evaporation method: an aqueous solution of $Na_2(hbdc)\cdot H_2O$ (0.3 mmol in 5 mL) was added to an aqueous solution of a lanthanide chloride (0.2 mmol in 5 mL). The mixture was stirred for 1 day. Precipitation occurred. The mixture was filtrated and the filtrate was evaporated at ambient temperature for a few days. Transparent single-crystals suitable for single-crystal X-ray diffraction were obtained (structural families **F1** and **F5**).

(iii) Diffusion through gel method: two different crystal structures (**F3** and **F6**) have been obtained by slow diffusion through gel media of a lanthanide chloride (0.25 mmol in 10 mL of water) and $Na_2(hbdc)\cdot H_2O$ (0.25 mmol in 10 mL of water) in U-shaped tubes. The gel (TMOS) has been used in 7.5% concentration (weight percent). After a few weeks, transparent single-crystals suitable for X-ray diffraction were obtained.

X-ray diffraction

Powder X-ray diffraction diagrams were collected with a Panalytical X'Pert Pro diffractometer equipped with a X'Celerator detector. Typical recording conditions were: 45 kV, 40 mA, Cu K_α radiation (λ = 1.542 Å), θ/θ mode. Simulated patterns from crystal structure were produced with PowderCell and WinPLOTR programs.[1-3]

Single crystals were mounted on a Bruker D8 Venture diffractometer. Crystal data collection were performed at 150 K with Mo K_α radiation (λ = 0.70713 Å) except for **F1** that has been done at room temperature. Crystal structures were solved, using SIR 97,[4] by direct methods. They were refined, using SHELX-2017[5] with the aid of WINGX program.[6-7] All non-hydrogen atoms were refined anisotropically. Hydrogen atoms that have been located were located at ideal positions. Absorption corrections were performed using the facilities of WINGX program.[8] In all crystal structure the ligand is disordered. Indeed this fat ligand can adopt two conformation rotated by 180° from each other. In all cases, the two conformations have been set to 50%. Full details of the crystal structures have been deposited with the Cambridge Crystallographic Data Centers under the depositary numbers CCDC-1913183 for $[Pr(Hhbdc)(hbdc)\cdot 9H_2O]_\infty$ **(F1)**, CCDC-1913130 for $[Sm_2(hbdc)_3(H_2O)_6\cdot 4H_2O]_\infty$ **(F2)**, CCDC-1913137 for $[Y_2(hbdc)_3(H_2O)_4\cdot 4H_2O]_\infty$ **(F3)**, CCDC-1913124 for $[Tb(Hhbdc)(hbdc)(H_2O)_3\cdot H_2O]_\infty$ **(F4),** CCDC-1913145 for $[Gd_2(hbdc)_3(H_2O)_8\cdot 6H_2O]_\infty$ **(F5)** and CCDC-1913142 for $[Gd_2(hbdc)_3(H_2O)_8\cdot 2H_2O]_\infty$ **(F6)**.

Thermal analyses.

Thermal analyses have been performed using a Perkin Elmer Pyris Diamond TGA/TDA, between 20°C and 950°C in platinum crucibles under N_2 atmosphere.

Electron dispersive spectroscopy.

EDS measurements have been performed with a Hitachi TM-1000, Tabletop Microscope version 02.11 (Hitachi High-Technologies, Corporation Tokyo Japan) with EDS analysis system (SwiftED-TM, Oxford Instruments Link INCA). Samples were deposited on carbon discs. Reproducibility of the elemental analyses has been checked by repeating the measurements several times. These experiments confirm the homogeneity of the samples.

Optical measurements.

Solid-state emission and excitation spectra have been measured on a Horiba Jobin-Yvon Fluorolog III fluorescence spectrometer equipped with a Xe lamp 450 W, a UV-Vis photomultiplier (Hamamatsu R928, sensitivity 190 - 860 nm) and an IR-photodiode cooled by liquid nitrogen (InGaAs, sensitivity 800 – 1600 nm). Quantum yield measurements were performed using a F-3018 Jobin-Yvon integrating sphere ($\Phi = (E_c - E_a)/(L_a - L_c)$ with E_c being the integrated emission spectrum of the sample, E_a the integrated "blank" emission spectrum, L_a the "blank" absorption and L_c the sample absorption at the excitation wavelength). The emission/excitation spectra and quantum yield recordings were realized on powder samples introduced in cylindrical quartz cells of 0.7 cm diameter and 2.4 cm height, which were placed directly inside the integrating sphere, or on powder samples pasted on copper plates with silver glue. The luminescence of the Gd-microcrystalline powders placed

in quartz capillary tubes has been measured at 77 K (Dewar + liquid nitrogen). Longest luminescence decays ($\tau > 10$ µs) have also been measured at room-temperature using this apparatus with a Xenon flash lamp (phosphorescence mode). Shortest luminescence decays ($\tau < 10$ µs) were measured directly with the fluorescence spectrometer coupled with an additional TCSPC module (Time-Correlated-Single-Photon-Counting) and a 320 nm pulsed Delta-Diode. Lifetimes and quantum yields are averages of three independent determinations.

Comparative solid-state luminescent spectra have been measured on the same fluorimeter on powders samples shaped into pellets. Spectra were recorded between 450 and 725 nm under identical operating conditions and without turning the lamp off to ensure a valid comparison between the emission spectra.

Appropriate filters were used to remove the residual excitation laser light, the Rayleigh scattered light and associated harmonics from spectra. All spectra were corrected for the instrumental response function.

Luminance of the samples expressed in $cd.m^{-2}$ have been measured with a Gigahertz-Optik X1-1 optometer with an integration time of 200 ms on 1.5 cm^2 pellets under UV irradiation ($\lambda_{exc} = 312$ nm). The intensity of the UV flux at sample location, 0.68(1) $mW.cm^{-2}$, has been measured with a VilberLourmat VLX-3W radiometer. $[Tb_2(bdc)_3 \cdot 4H_2O]_\infty$ where bdc^{2-} stands for terephthalate was used as a standard. Its luminance is 98(3) $cd.m^{-2}$ under these operating conditions ($\lambda_{exc} = 312$ nm; flux = 0.68(1) $mW.cm^{-2}$).[9]

The CIE (Commission Internationale de l'Eclairage) (x, y) emission color coordinates[10-11] were measured with a MSU-003 colorimeter (Majantys) equipped with the PhotonProbe 1.6.0 Software (Majantys). Color measurements: 2°, CIE 1931, step 5 nm, under 312 nm UV light. $X = k \times \int_{380nm}^{780nm} I_\lambda \times x_\lambda$, $Y = k \times \int_{380nm}^{780nm} I_\lambda \times y_\lambda$ and $Z = k \times \int_{380nm}^{780nm} I_\lambda \times z_\lambda$ with k constant for the measurement system, I_λ sample spectrum intensity wavelength depending, x_λ, y_λ, z_λ trichromatic values x = X/(X+Y+Z), y = Y/(X+Y+Z) and z = Z/(X+Y+Z). Mean xyz values are given for each sample, which act as light sources (luminescent samples). Standards from Phosphor Technology used, calibrated at 312 nm: red phosphor Gd_2O_2S:Eu (x = 0.667, y = 0.330) and green phosphor Gd_2O_2S:Tb (x = 0.328, y = 0.537).

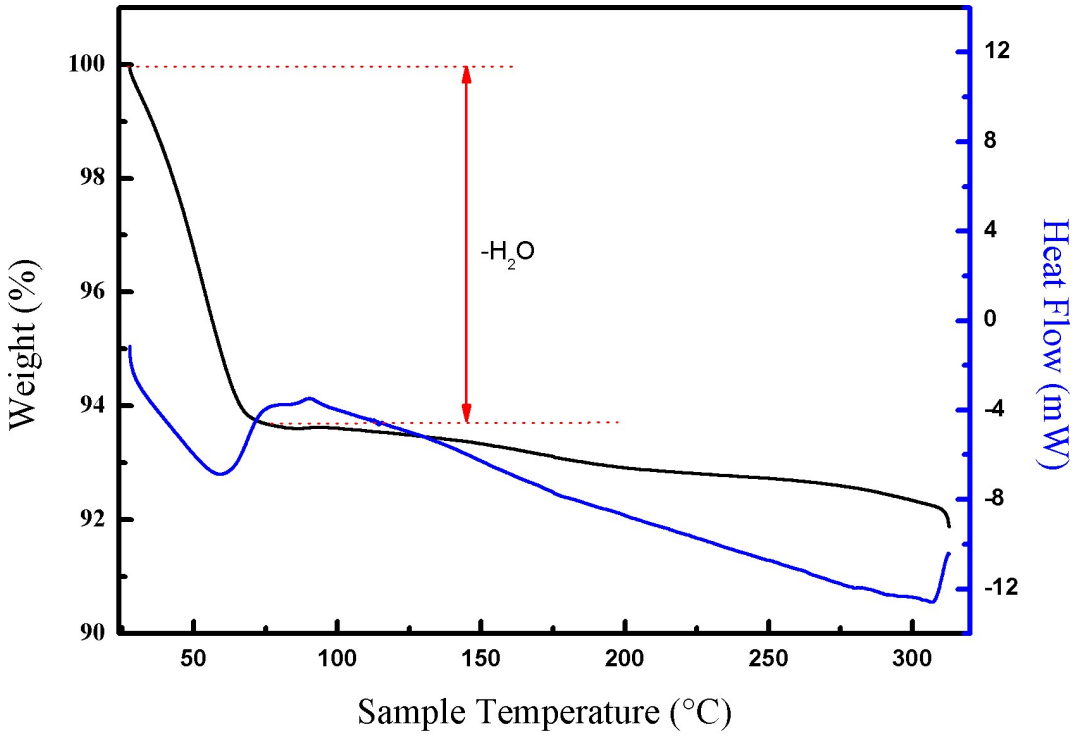

Figure S1. TG/TD analysis of $Na_2(hbdc)\cdot H_2O$ under N_2 flux from room temperature to 300°C.

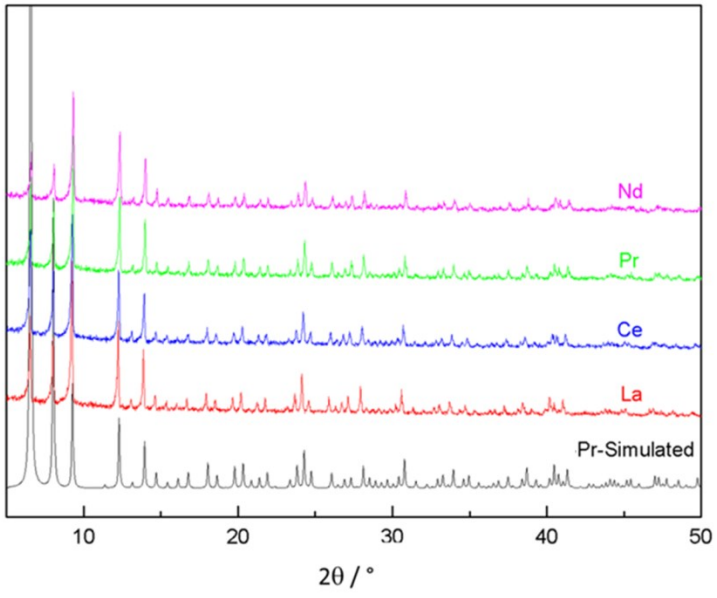

Figure S2. Experimental powder X-ray diffraction diagrams of $[Ln(Hhbcd)(hbdc)\cdot 9H_2O]_\infty$ with Ln = La-Nd (**F1**) and simulated pattern calculated from the crystal structure of $[Pr(Hhbcd)(hbdc)\cdot 9H_2O]_\infty$.

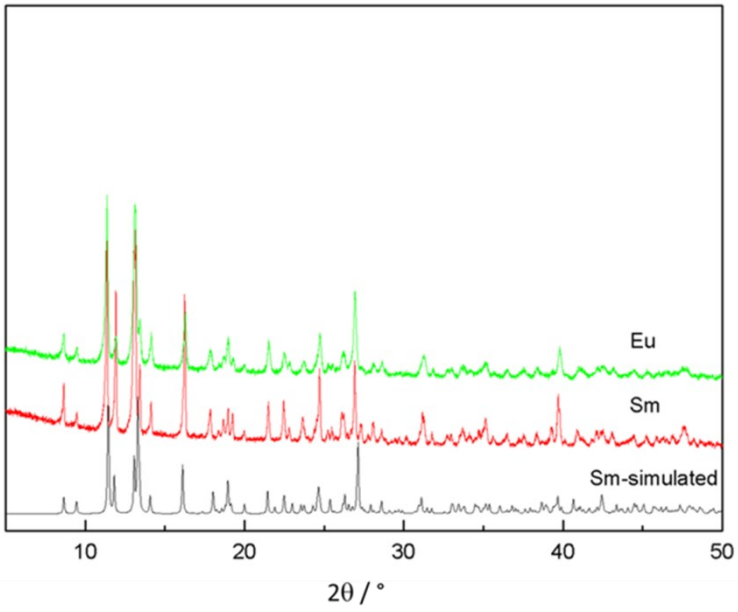

Figure S3. Experimental powder X-ray diffraction diagrams of $[Ln_2(hbdc)_3(H_2O)_6{\cdot}4H_2O]_\infty$ with Ln = Sm-Eu (**F2**) and simulated pattern calculated from the crystal structure of $[Sm_2(hbdc)_3(H_2O)_6{\cdot}4H_2O]_\infty$.

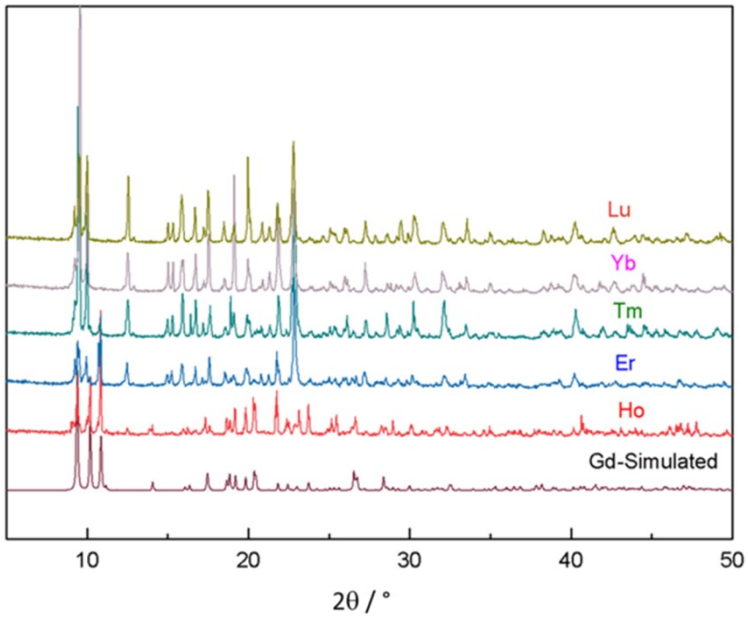

Figure S4. Experimental powder X-ray diffraction diagrams of $[Ln_2(hbdc)_3(H_2O)_4{\cdot}4H_2O]_\infty$ with Ln = Ho-Lu (**F3**) and simulated pattern calculated from the crystal structure of $[Gd_2(hbdc)_3(H_2O)_4{\cdot}4H_2O]_\infty$.

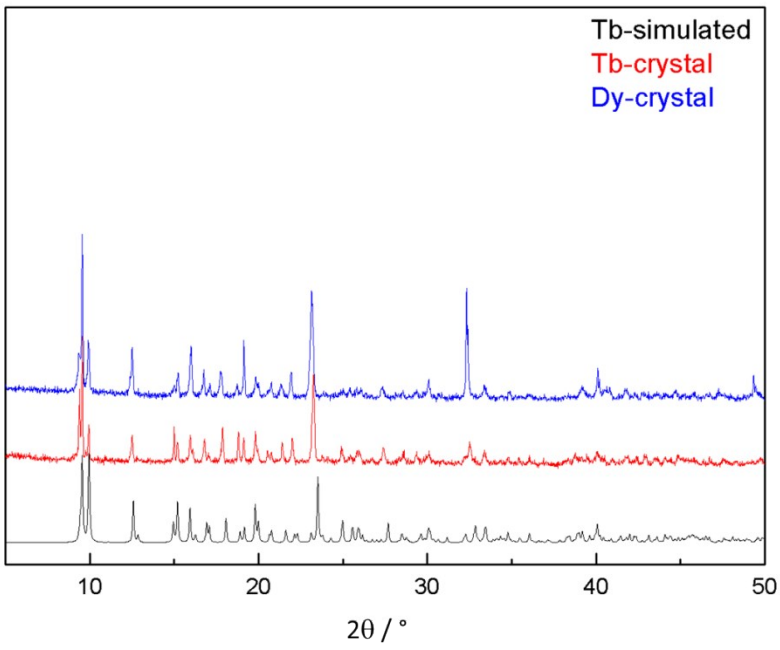

Figure S5. Experimental powder X-ray diffraction diagrams of $[Ln(Hhbdc)(hbdc)(H_2O)_3 \cdot H_2O]_\infty$ with Ln = Tb-Dy (**F4**) and simulated pattern calculated from the crystal structure of $[Tb_2(hbdc)_3(H_2O)_4 \cdot 4H_2O]_\infty$.

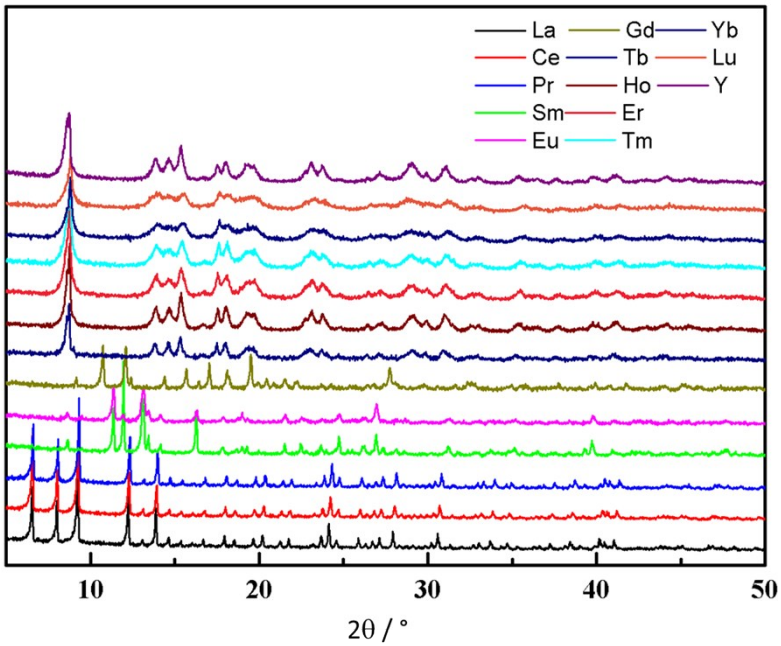

Figure S6. Experimental powder X-ray diffraction diagrams of the microcrystalline powder obtained by mixing a lanthanide chloride and the di-sodium salt of 2-hydroxy-terephthalic acid.

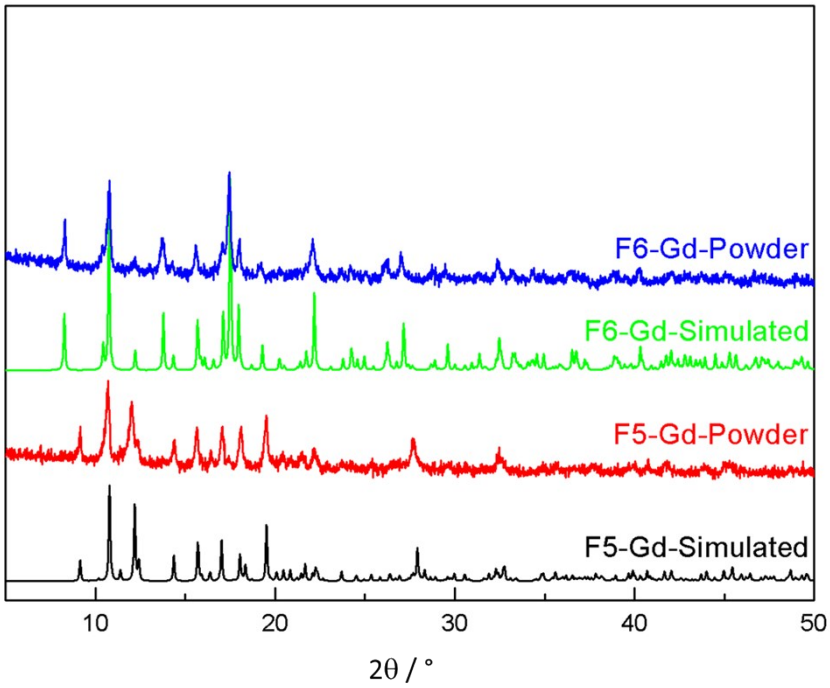

Figure S7. Experimental powder X-ray diffraction diagrams of the microcrystalline powders of $[Gd_2(hbdc)_3(H_2O)_8{\cdot}6H_2O]_\infty$ (**F5**) and $[Gd_2(hbdc)_3(H_2O)_8{\cdot}2H_2O]_\infty$ (**F6**) together with the simulated X-ray diffraction diagrams from the crystal structures.

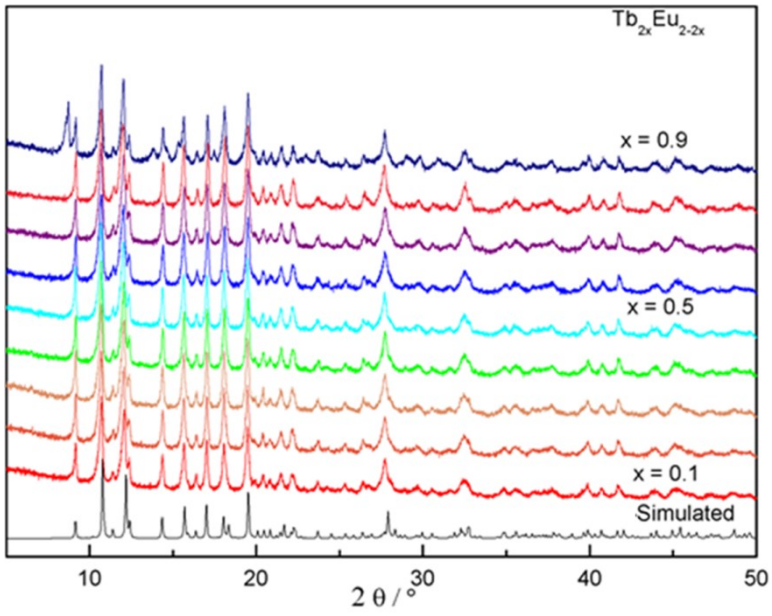

Figure S8. Experimental powder X-ray diffraction diagrams of $[Tb_{2x}Eu_{2-2x}(hbdc)_3(H_2O)_8{\cdot}6H_2O]_\infty$ ($0 \le x \le 1$) (Family **F5**) and simulated PXRD diagram of $[Gd_2(hbdc)_3(H_2O)_8{\cdot}6H_2O]_\infty$ (**F5**) based on its crystal structure.

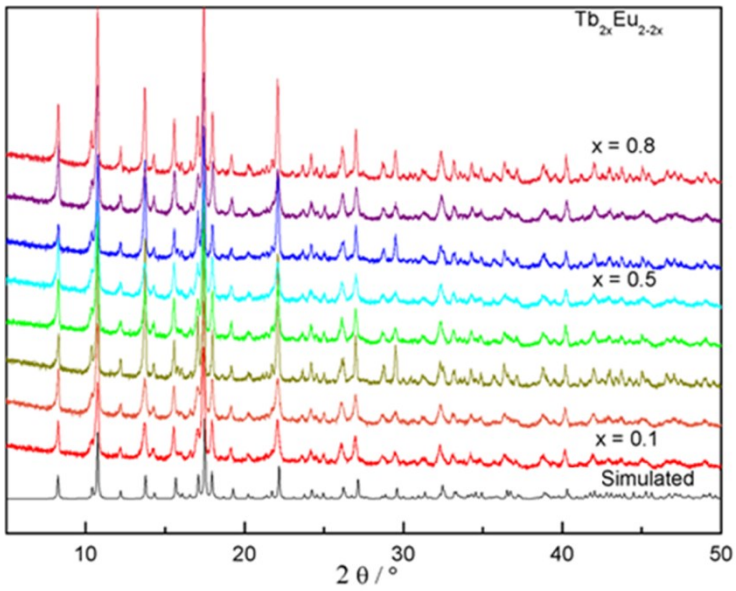

Figure S9. Experimental powder X-ray diffraction diagrams of $[Tb_{2x}Eu_{2-2x}(hbdc)_3(H_2O)_8{\cdot}2H_2O]_\infty$ with $0 \le x \le 0.8$ (Family **F6**) and simulated PXRD pattern of $[Gd_2(hbdc)_3(H_2O)_8{\cdot}2H_2O]_\infty$ (**F6**) based on its crystal.

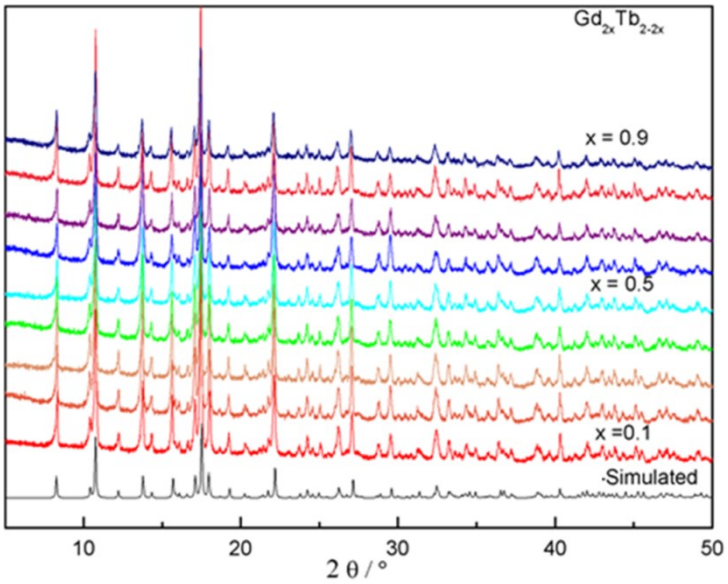

Figure S10. Experimental powder X-ray diffraction diagrams of $[Gd_{2x}Tb_{2-2x}(hbdc)_3(H_2O)_8{\cdot}2H_2O]_\infty$ with $0 \le x \le 0.9$ (Family **F6**) and simulated PXRD pattern of $[Gd_2(hbdc)_3(H_2O)_8{\cdot}2H_2O]_\infty$ (**F6**) based on its crystal.

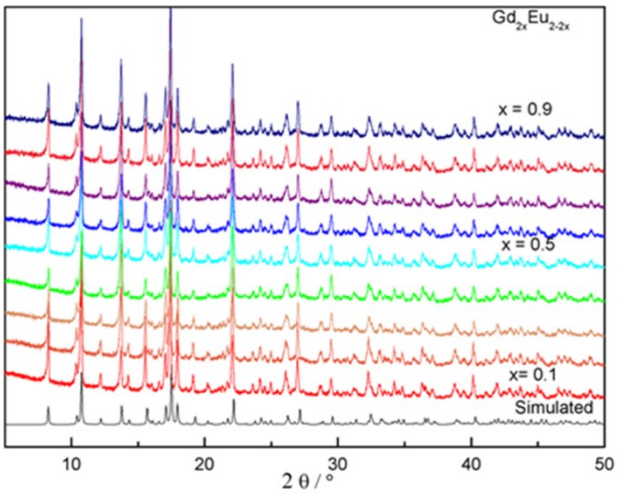

Figure S11. Experimental powder X-ray diffraction diagrams of $[Gd_{2x}Eu_{2-2x}(hbdc)_3(H_2O)_8{\cdot}2H_2O]_\infty$ with $0 \le x \le 0.9$ (Family **F6**) and simulated PXRD pattern of $[Gd_2(hbdc)_3(H_2O)_8{\cdot}2H_2O]_\infty$ (**F6**) based on its crystal.

Table S1. Relative metallic contents measured by EDS for $[Tb_{2x}Eu_{2-2x}(hbdc)_3(H_2O)_8{\cdot}6H_2O]_\infty$ ($0 \le x \le 1$) (**F5**), $[Tb_{2x}Eu_{2-2x}(hbdc)_3(H_2O)_8{\cdot}2H_2O]_\infty$ ($0 \le x \le 0.8$) (**F6**), $[Gd_{2x}Eu_{2-2x}(hbdc)_3(H_2O)_8{\cdot}2H_2O]_\infty$ ($0 \le x \le 0.9$) (**F6**) and $[Gd_{2x}Tb_{2-2x}(hbdc)_3(H_2O)_8{\cdot}2H_2O]_\infty$ ($0 \le x \le 0.8$) (**F6**)

$[Tb_{2x}Eu_{2-2x}(hbdc)_3(H_2O)_8{\cdot}6H_2O]_\infty$ (**F5**)

x	Tb %	Eu%
0.1	10(2)	90(2)
0.2	20(1)	80(1)
0.3	30(2)	70(2)
0.4	40(2)	60(2)
0.5	50(1)	50(1)
0.6	59(1)	41(1)
0.7	70(2)	30(2)
0.8	80(2)	20(2)

$[Tb_{2x}Eu_{2-2x}(hbdc)_3(H_2O)_8{\cdot}2H_2O]_\infty$ (**F6**)

x	Tb %	Eu%
0.1	10(2)	90(2)
0.2	20(2)	80(2)
0.3	31(2)	69(2)
0.4	40(2)	60(2)
0.5	49(2)	51(2)
0.6	60(2)	40(2)
0.7	71(1)	29(1)
0.8	80(2)	20(2)

$[Gd_{2x}Eu_{2-2x}(hbdc)_3(H_2O)_8{\cdot}2H_2O]_\infty$ (**F6**)

x	Gd %	Eu%
0.1	10(1)	90(1)
0.2	20(2)	80(2)
0.3	30(2)	70(2)
0.4	40(2)	60(2)
0.5	53(1)	47(1)
0.6	60(1)	40(1)
0.7	70(1)	30(1)
0.8	80(1)	20(1)
0.9	90(1)	10(1)

$[Gd_{2x}Tb_{2-2x}(hbdc)_3(H_2O)_8{\cdot}2H_2O]_\infty$ (**F6**)

x	Gd %	Tb %
0.1	10(1)	90(1)
0.2	20(1)	80(1)
0.3	30(1)	70(1)
0.4	40(1)	60(1)
0.5	51(2)	49(2)
0.6	60(2)	40(2)
0.7	70(2)	30(2)
0.8	80(1)	20(1)
0.9	89(1)	11(1)

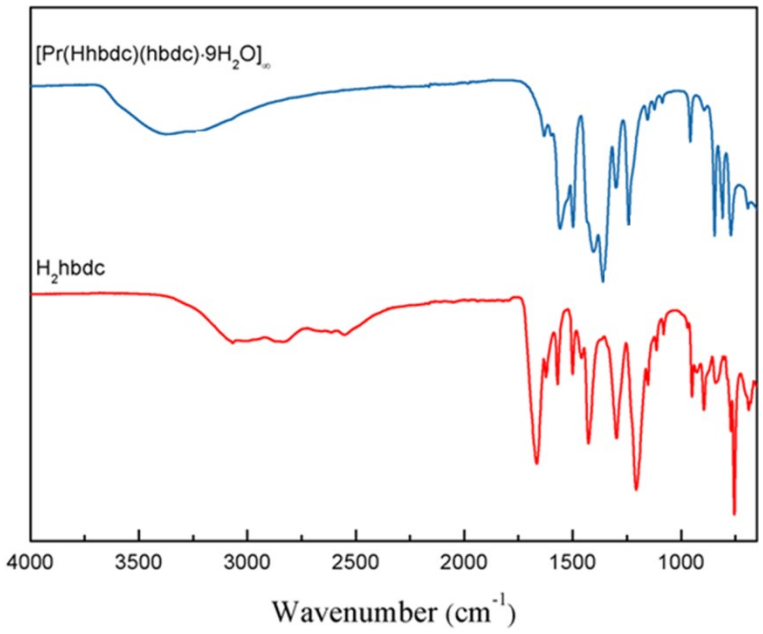

Figure S12. Solid-state IR spectra of $[Pr(Hhbdc)(hbdc)\cdot 9H_2O]_\infty$ (**F1**) and H_2hbdc.

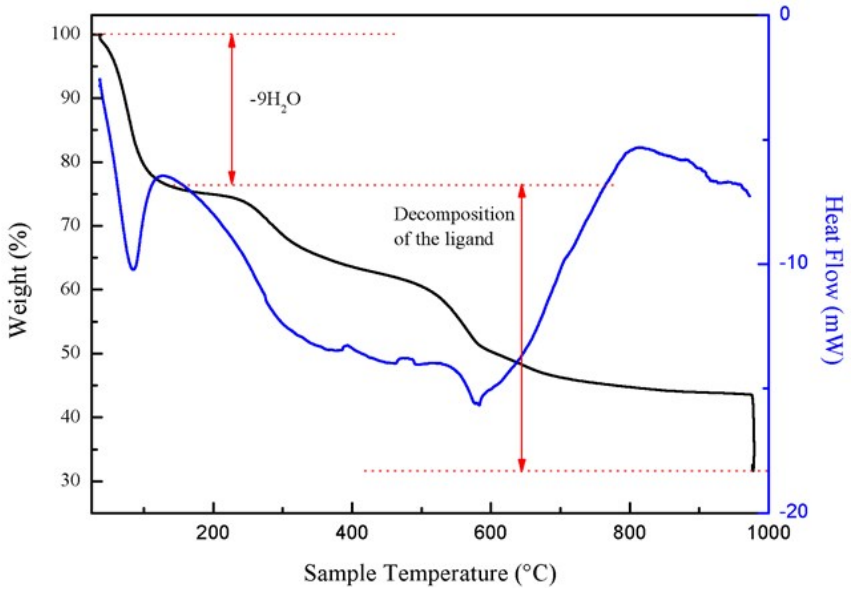

Figure S13. TGA/TDA curves for $[Pr(Hhbdc)(hbdc)\cdot 9H_2O]_\infty$ (**F1**).

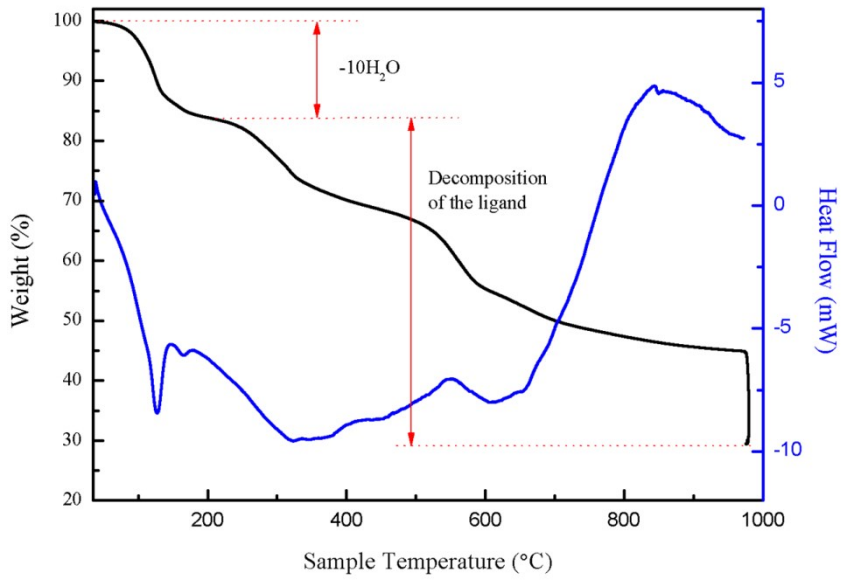

Figure S14. TGA/TDA curves for $[Sm_2(hbdc)_3(H_2O)_6{\cdot}4H_2O]_\infty$ (**F2**).

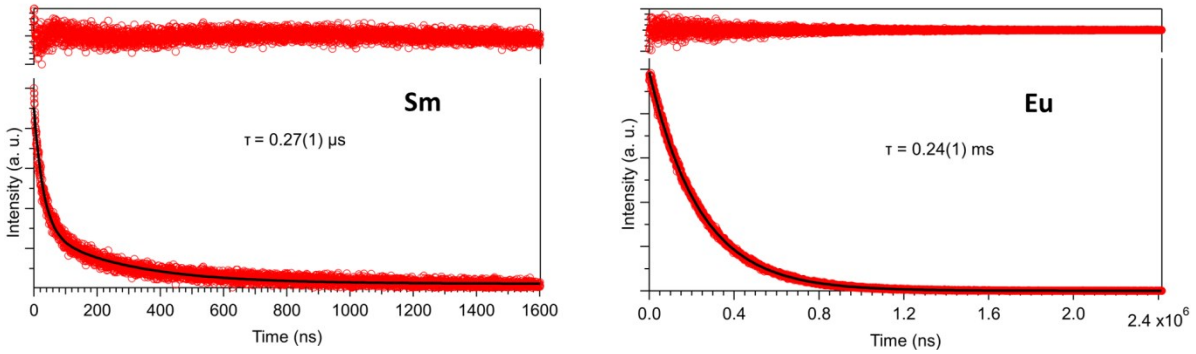

Figure S15. Luminescence decay curves at room temperature for $[Sm_2(hbdc)_3(H_2O)_6{\cdot}4H_2O]_\infty$ (**F2**) (left) and $[Eu_2(hbdc)_3(H_2O)_6{\cdot}4H_2O]_\infty$ (**F2**) (right).

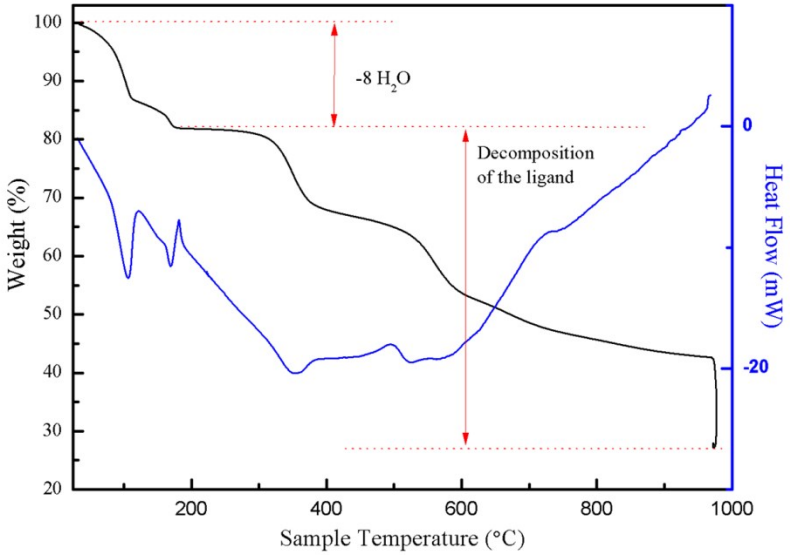

Figure S16. TGA/TDA curves for $[Y_2(hbdc)_3(H_2O)_4{\cdot}4H_2O]_\infty$ (**F3**).

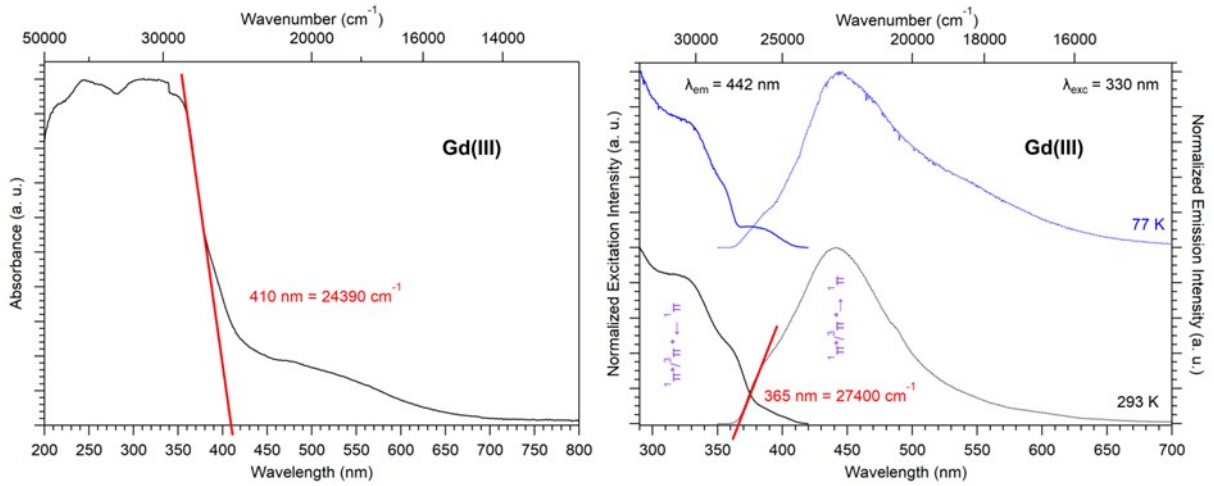

Figure S17. Solid-state absorption spectrum at 293 K (left), excitation and emission spectra at 77 K and 293 K (right) for $[Gd_2(hbdc)_3(H_2O)_4{\cdot}4H_2O]_\infty$ (**F3**).

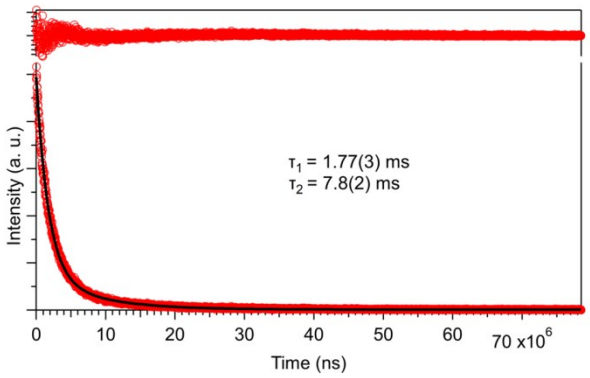

Figure S18. Luminescence decay curve of $[Gd_2(hbdc)_3(H_2O)_4{\cdot}4H_2O]_\infty$ (**F3**) at 77 K: τ_1 = 1.77(3) ms and τ_2 = 7.8(2) ms with λ_{ex} = 330 nm (bi-exponential fit).

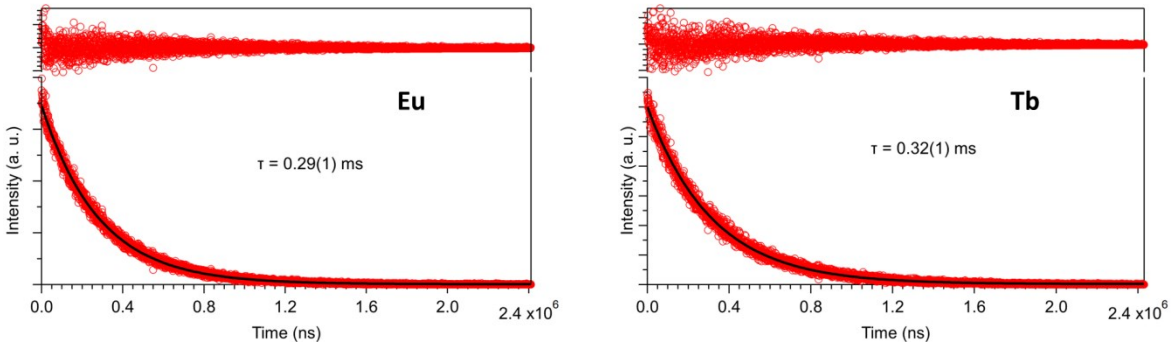

Figure S19. Luminescence decay curve at room temperature of $[Eu_2(hbdc)_3(H_2O)_4{\cdot}4H_2O]_\infty$ (**F3**) and $[Tb_2(hbdc)_3(H_2O)_4{\cdot}4H_2O]_\infty$ (**F3**).

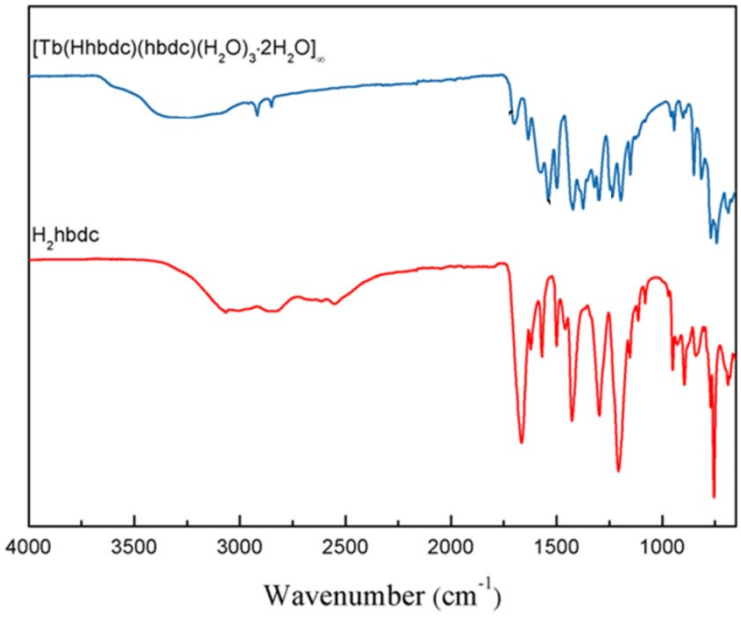

Figure S20. Solid-state IR spectra of $[Tb(Hhbdc)(hbdc)(H_2O)_3{\cdot}H_2O]_\infty$ (**F4**) and H_2hbdc

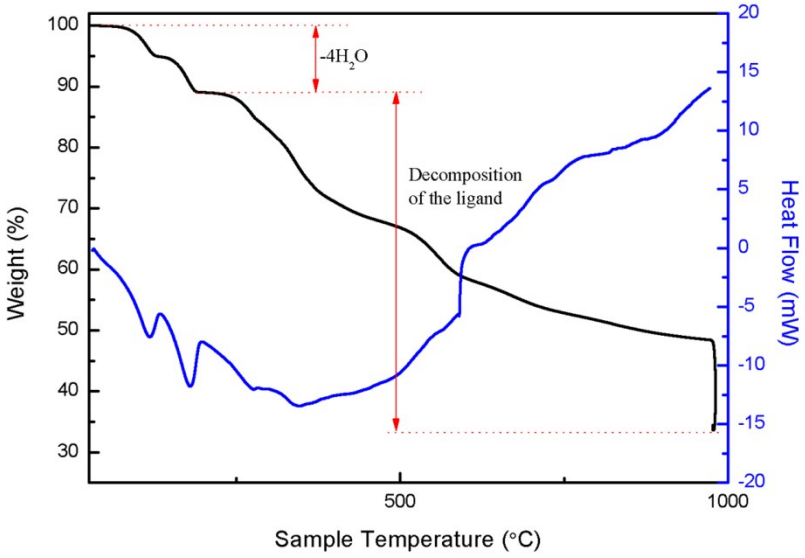

Figure S21. TGA/TDA curves for $[Tb(Hhbdc)(hbdc)(H_2O)_3 \cdot H_2O]_\infty$ (**F4**).

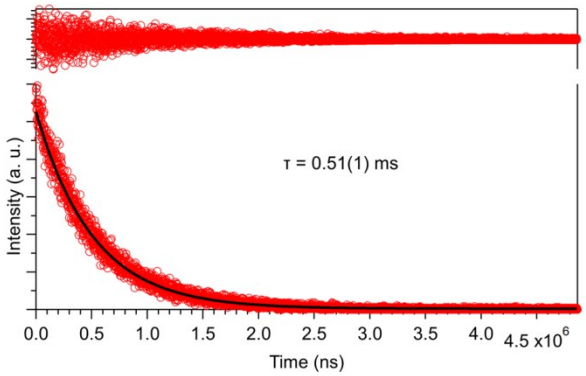

Figure S22. Luminescence decay curve at room temperature of $[Tb(Hhbdc)(hbdc)(H_2O)_3 \cdot H_2O]_\infty$ (**F4**).

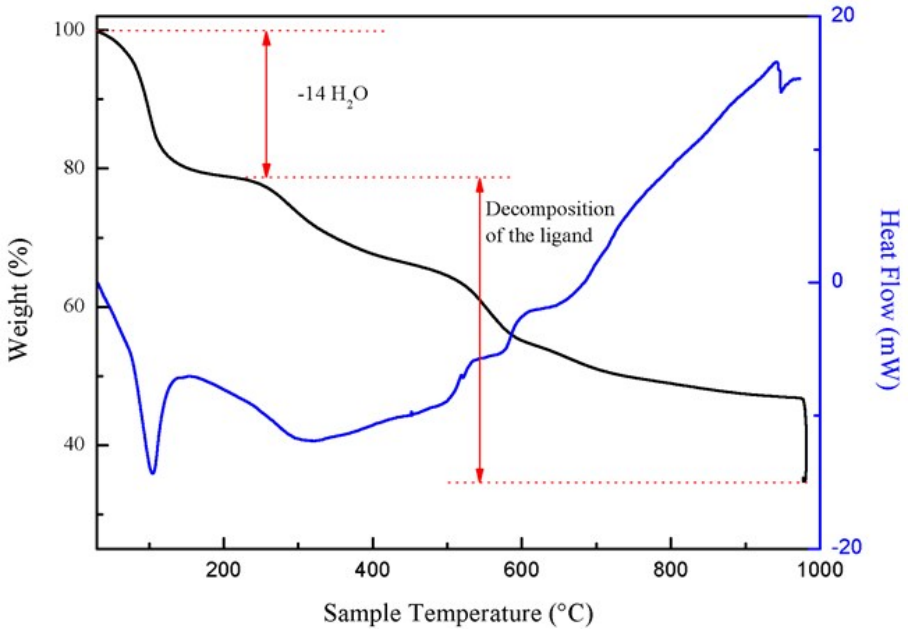

Figure S23. TG/TDA curves for $[Gd_2(hbdc)_3(H_2O)_8{\cdot}6H_2O]_\infty$ (**F5**).

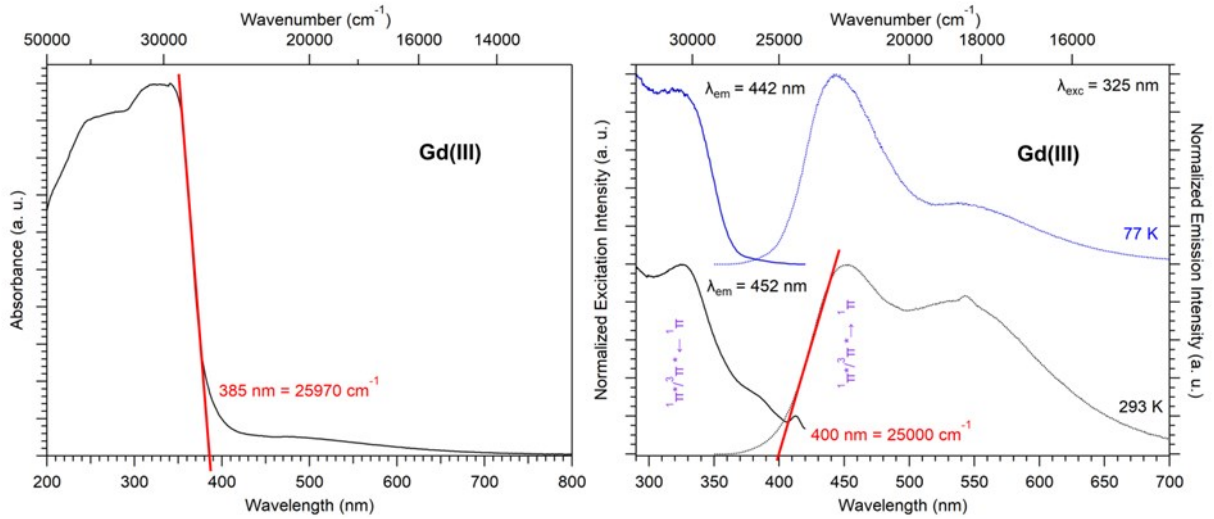

Figure S24. Solid-state absorption spectrum at 293 K (left), excitation and emission spectra at 77 K and 293 K (right) for $[Gd_2(hbdc)_3(H_2O)_8{\cdot}6H_2O]_\infty$ (**F5**).

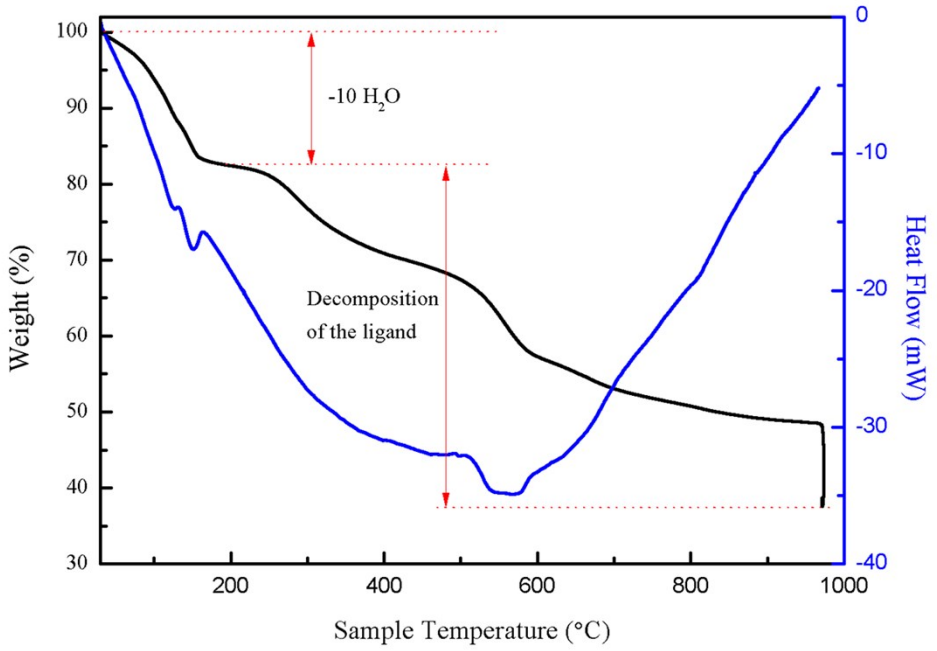

Figure S25. TGA/TDA curves of $[Gd_2(hbdc)_3(H_2O)_8{\cdot}2H_2O]_\infty$ (**F6**).

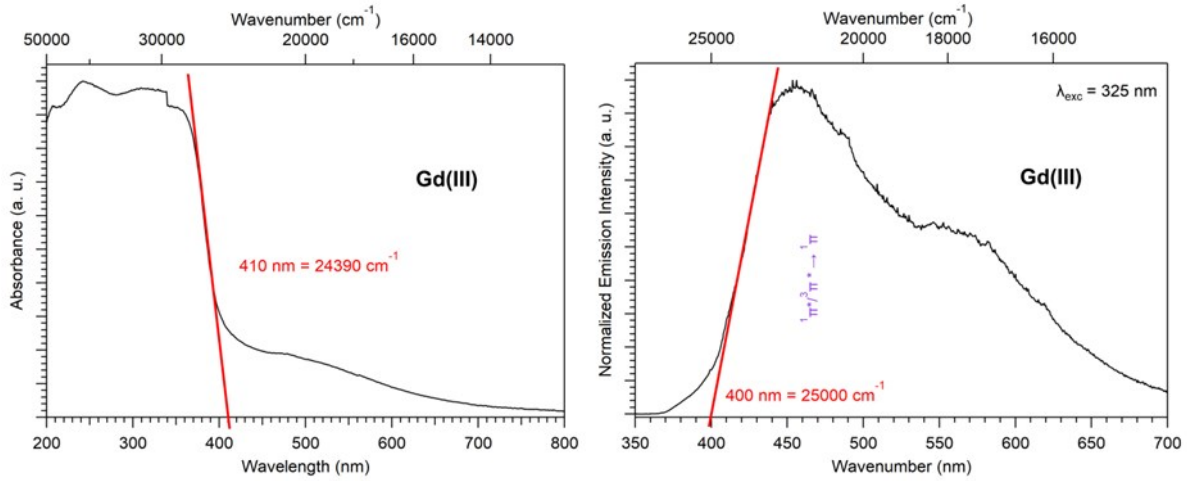

Figure S26. Solid-state absorption spectrum at 293 K (left) and emission spectrum at 77 K (right) for $[Gd_2(hbdc)_3(H_2O)_8{\cdot}2H_2O]_\infty$ (**F6**).

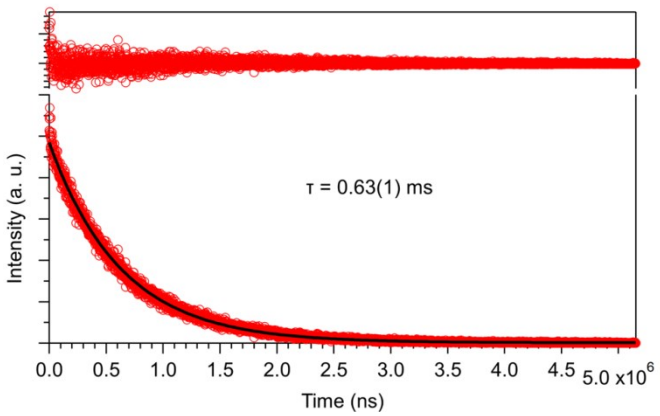

Figure S27. Luminescence decay curve at room temperature of $[Tb_2(hbdc)_3(H_2O)_8{\cdot}2H_2O]_\infty$ (**F6**).

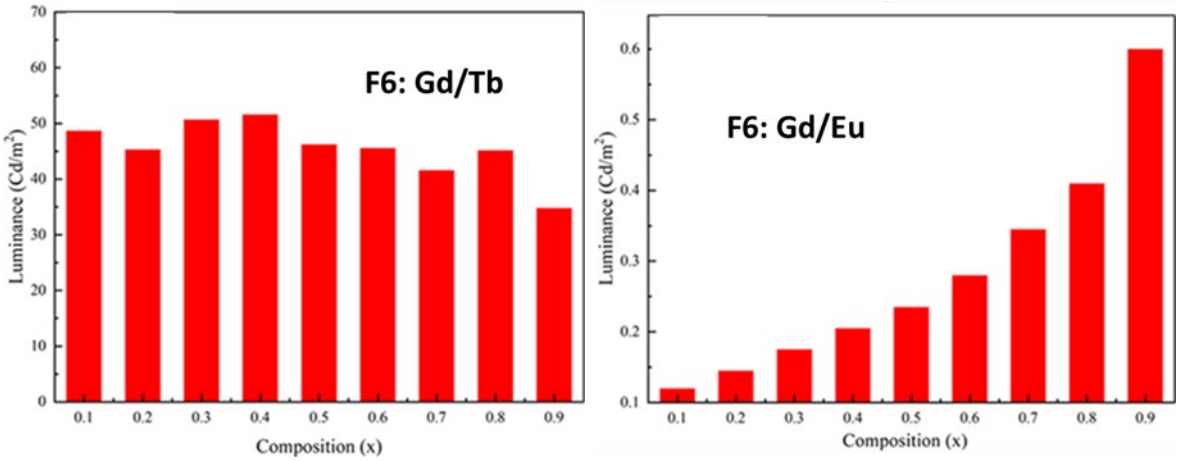

Figure S28. Luminance measurements under UV irradiation (312 nm, flux = 0.68(1) mW.cm^{-2}) of $[Gd_{2x}Tb_{2-2x}(hbdc)_3(H_2O)_8{\cdot}2H_2O]_\infty$ (**F6**) (left) and $[Gd_{2x}Eu_{2-2x}(hbdc)_3(H_2O)_8{\cdot}2H_2O]_\infty$ (**F6**) (right) *versus* x ($0 < x < 1$) at room temperature.

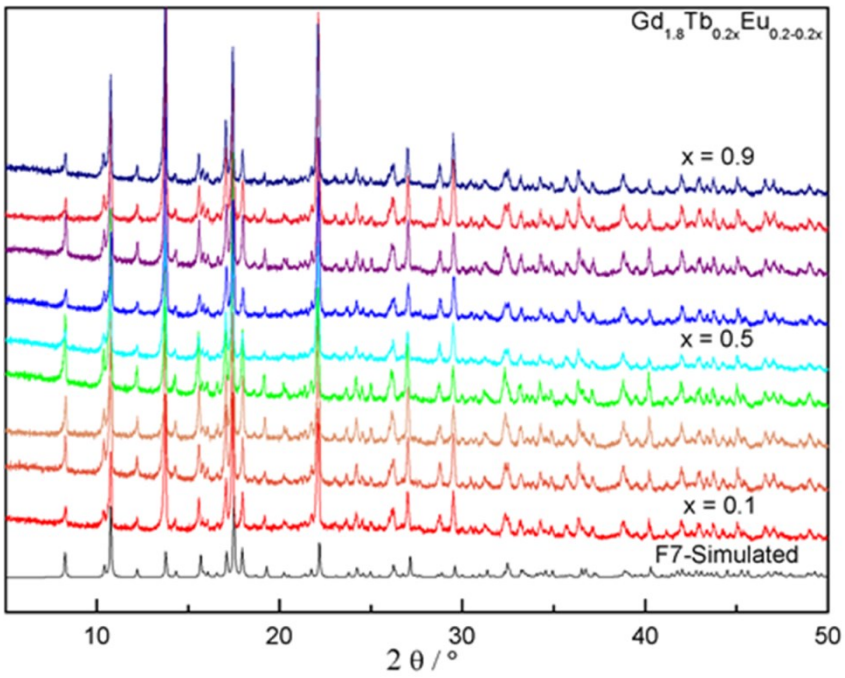

Figure S29. Experimental powder X-ray diffraction diagrams of $[Gd_{1.8}Tb_{0.2x}Eu_{0.2-0.2x}(hbdc)_3(H_2O)_8{\cdot}2H_2O]_\infty$ with $0 \le x \le 0.9$ (Family **F6**) and simulated PXRD pattern of $[Gd_2(hbdc)_3(H_2O)_8{\cdot}2H_2O]_\infty$ (**F6**) based on its crystal structure.

Table S2. Relative metallic contents measured by EDS for $[Gd_{1.8}Tb_{0.2x}Eu_{0.2-0.2x}(hbdc)_3]_\infty$ $(0 \le x \le 0.9)$ (**F6**)

x	Gd %	Tb%	Eu%
0.1	90(2)	1(1)	9(1)
0.2	90(2)	2(1)	8(2)
0.3	90(1)	3(1)	7(1)
0.4	90(2)	4(2)	6(1)
0.5	89(1)	6(1)	5(1)
0.6	90(1)	6(1)	4(1)
0.7	90(2)	7(2)	3(1)
0.8	90(2)	8(2)	2(1)
0.9	90(2)	9(2)	1(1)

REFERENCES

1. Kraus, W.; Nolze, G., POWDER CELL - A program for the representation and manipulation of crystal structures and calculation of the resulting X-ray powder patterns. *J. Appl. Crystallogr.* **1996,** *29*, 301-303.
2. Roisnel, T.; Rodriguez-Carjaval, J., A Window Tool for Powder Diffraction Patterns Analysis. *J. Mater. Sci. Forum* **2001,** *378*, 118-123.
3. Roisnel, T.; Rodriguez-Carjaval, J., WinPLOTR : a windows tool for powder diffraction pattern analysis. *Materials Science Forum, Proceedings of the Seventh European Powder Diffraction Conference (EPDIC 7)* **2000**, 118-123.
4. Altomare, A.; Burla, M. C.; Camalli, M.; Carrozzini, B.; Cascarano, G.; Giacovazzo, C.; Guagliardi, A.; Moliterni, A. G. G.; Polidori, G.; Rizzi, A. C., EXPO: a program for full powder pattern decomposition and crystal structure solution. *J. Appl. Crystallogr.* **1999,** *32*, 339-340.
5. Sheldrick, G. M.; Schneider, T. R., SHELXL : High-Resolution Refinement. *Macromol. Crystallogr. B* **1997**, 319-343.
6. Farrugia, L. J., WinGX and ORTEP for Windows: an update. *J. Appl. Crystallogr.* **2012,** *45*, 849-854.
7. Farrugia, L. J., WinGX suite for smallmolecule single-crystal crystallography. *J. Appl. Crystallogr.* **1999,** *32*, 837-838.
8. Sluis, P.; Spek, A. L., BYPASS: an Effective method for the refinement of crystal structures containing disordered solvent regions. *Acta Crystallogr. A* **1990,** *A46*, 194-201.
9. Haquin, V.; Etienne, M.; Daiguebonne, C.; Freslon, S.; Calvez, G.; Bernot, K.; Le Polles, L.; Ashbrook, S. E.; Mitchell, M. R.; Bünzli, J. C. G.; Guillou, O., Color and brightness tuning in hetero-nuclear lanthanide teraphthalate coordination polymers. *Eur. J. Inorg. Chem.* **2013**, 3464-3476.
10. CIE, *International Commission on Illumination - Technical report*. CIE: **1995;** Vol. 13-3, p 16.
11. Wyszecki, G., Colorimetry. In *Handbook of Optics*, Driscoll, W. G.; Vaughan, W., Eds. Mac Graw-Hill Book Company: New-York, **1978**, p 1-15.